Composition-dependent transition from spin glass to ferrimagnet in $CaLa_2Ni_{2-x}Cu_xWO_9$ ($0 \leq x \leq 0.5$)

Chun-Mann Chin, Simon J. Cassidy, Emily C. Hunter and Peter D. Battle*

Inorganic Chemistry Laboratory,

University of Oxford,

South Parks Road,

Oxford,

OX1 3QR,

U. K.

* Corresponding author

Email address: peter.battle@chem.ox.ac.uk

Abstract

Polycrystalline samples of the monoclinic perovskites $CaLa_2Ni_{2-x}Cu_xWO_9$ (x = 0.25 and 0.5) have been prepared and characterised by neutron diffraction and magnetometry. The Ni^{2+}, Cu^{2+} and W^{6+} cations are partially ordered over two crystallographically-distinct six-coordinate sites such that one is ~63 % occupied by W^{6+} and both are occupied by Ni^{2+} and Cu^{2+} in a ratio of (2-x):x. The composition x = 0.25 behaves as a spin glass below 35 K whereas x = 0.5 is ferrimagnetic below 120 K with an ordered moment of 0.774(5) μ_B per magnetic cation. The atomic moments order in a G-type pattern and the imbalance in the number of magnetic cations on the two sites results in a net magnetisation.

Keywords: Perovskite, spin glass, ferrimagnet, neutron diffraction

Introduction

Our recent studies on triple perovskites having the general formula $(A,A')_3B_2B'O_9$ have identified relaxor ferromagnets ($La_3Ni_2TaO_9$ [1]), ferrimagnets ($LaSr_2Cr_2SbO_9$ [2]) and spin glasses ($La_3Ni_2NbO_9$ [3]). The difference in the behaviour of the two Ni^{2+}-containing oxides was ascribed to the energy difference between the empty 4*d* orbitals of Nb^{5+} and the 5*d* orbitals of Ta^{5+} [1]. As a consequence of this energy difference the degree of mixing between the *d* orbitals and the anion 2*p* levels will differ and hence the strength of magnetic superexchange coupling along pathways which include the pentavalent cation will vary. It was proposed that changes in the relative strengths of these interactions and those of the other superexchange interactions that are present can result in the observation of different magnetic behaviour. These compounds usually adopt a well-known [4, 5] monoclinic structure, often referred to as the double-perovskite structure, in which the *d* block cations are accommodated on two crystallographically-distinct, six-coordinate sites that alternate through the structure and are

thus present in equal numbers. The *B* and *B*' cations show partial long-range ordering over the two available sites such that one site is ~100 % occupied by *B* whereas the other is ~33 % and ~66 % occupied by *B* and *B*', respectively. There is no long-range ordering in the distribution of *B* and *B*' over this mixed site although there is evidence of short-range ordering in $La_3Ni_2SbO_9$ [6]. When this cation ordering pattern is present the superexchange interactions most likely to be modified by changes in the degree of involvement of the pentavalent cation are the pseudo-linear interaction between Ni^{2+} cations $2a_p$ apart and the 90 º interaction between those $\sqrt{2}a_p$ apart, where a_p is the unit cell parameter of the aristotype primitive-cubic perovskite. The interaction between nearest-neighbour cations separated by a distance a_p will not be affected.

In the case of $La_3Ni_2NbO_9$ the frustration caused by the presence of competing interactions leads to the formation of a spin glass phase below 29 K, although the positive Weiss temperature, θ_W = 137 K suggests that strong, short-range interactions are present. It has been shown [7] that the partial replacement of Ni^{2+} by Cu^{2+} in $La_3Ni_2NbO_9$ relieves the frustration and leads to the formation of a ferrimagnetic phase, although no detailed explanation of this behaviour is currently available. We describe below the consequences of making the same substitution into another spin glass, $CaLa_2Ni_2WO_9$ [8].

Experimental

Polycrystalline samples (~2 g) of $CaLa_2Ni_{2-x}Cu_xWO_9$ (x = 0.25 and 0.5), were prepared using the traditional ceramic method. Stoichiometric amounts of $CaCO_3$, NiO, CuO, WO_3 and pre-dried La_2O_3 (Alfa Aesar, >99.95 %) were mixed and ground thoroughly in an agate mortar and pestle. The mixtures were first heated at 800 °C as loose powders in alumina crucibles. They were then reground and pelletised before being heated at temperatures of up 1200 °C for 15 (x = 0.25) or 10 days (x = 0.5).

X-ray powder diffraction (XRPD) patterns of the reaction products were collected at room temperature on a PAN'alytical Empyrean diffractometer using Cu $K_{\alpha 1}$ radiation. Data were collected over the angular range $15 \leq 2\theta/° \leq 125$ with a step–size, $\Delta 2\theta$, of 0.0066° in an experiment that lasted 9 hours. The Rietveld method [9], as implemented in the GSAS program suite [10], was employed to analyse the data. A shifted Chebyshev function was used to model the background level.

XRPD is unable to distinguish effectively between Ni^{2+} and Cu^{2+} and neutron powder diffraction (NPD) was therefore used to identify any difference in the site preferences of these two cations, and also to investigate further the magnetic behaviour observed at low temperature. NPD data were collected on the WISH [11] time-of-flight diffractometer at the ISIS spallation source at selected temperatures in the range $1.6 \leq T/K \leq 300$. Each sample was loaded into a cylindrical vanadium can and mounted in an Oxford Instruments cryostat when data were to be collected below room temperature. The data collected on detector banks 2-9 were refined simultaneously using the Rietveld method as implemented in the program TOPAS [12]. The scattering angles for the different detector banks are as follows: banks 2/9, 58˚; banks 3/8, 90˚; banks 4/7, 122˚ and banks 5/6, 153˚. Data were collected for 1 hour on each sample at 1.6 K and room temperature. Additional data sets were collected for 15 minutes at intermediate temperatures selected after consideration of the results of the magnetic measurements described below.

The magnetic properties of $CaLa_2Ni_{2-x}Cu_xWO_9$ (x = 0.25 and 0.5) were investigated using a SQUID magnetometer. A known mass (~40 mg) of each sample was first cooled to 2 K in the absence of a magnetic field (Zero-Field Cooling, ZFC). The sample magnetisation was then measured on warming through the temperature range $2 \leq T/K \leq 300$ in a magnetic field of 100 Oe. A second data set was collected after the sample had been cooled to 2 K in the measuring field (Field Cooling, FC). The field dependence of the magnetisation was measured at 5, 150

and 220 K as the field was cycled through the range $-50 \leq H/\text{kOe} \leq 50$. In the case of $CaLa_2Ni_{1.75}Cu_{0.25}WO_9$ data were also collected at 25 K. The ac susceptibility of each sample was measured in an oscillating field of amplitude 3.5 Oe at frequencies, ω, of 1, 10, 100 and 1000 Hz. In each case the temperature range of these measurements was dictated by the transition temperature observed in the dc measurement.

Results

Preliminary Rietveld analysis of the XRPD patterns suggested the principal phase in both samples is a monoclinic (space group $P2_1/n$), perovskite-related material with $a \sim b \sim \sqrt{2}a_p$, $c \sim 2a_p$ and $\beta \sim 90°$ where a_p is the cell parameter of a primitive cubic perovskite.

The temperature dependence of the dc molar magnetic susceptibility of $CaLa_2Ni_{2-x}Cu_xWO_9$ (x = 0.25 and 0.5) is shown in Figure 1. The data show a marked dependence on composition. For x = 0.25, the ZFC susceptibility overlies the FC susceptibility at T > 35 K and both reach a relatively sharp maximum at ~35 K, T_{MAX}. The gradients of χ_{ZFC} and χ_{FC} differ below that temperature, with $\frac{d\chi_{ZFC}}{dT}$ being the more positive; χ_{FC} is independent of temperature below 15 K. In sharp contrast, the susceptibility of $CaLa_2Ni_{1.5}Cu_{0.5}WO_9$ increases markedly on cooling below 150 K and hysteresis is apparent below 110 K. At low temperatures the magnitude of χ_{FC} is an order of magnitude higher than in the case of the more Ni-rich composition. In both cases $\chi^{-1}(T)$ is linear above ~200 K, consistent with both samples being Curie paramagnets above that temperature. The molar Curie constant, C_m, and the Weiss temperature, θ_W, were derived from fitting the data collected over the temperature range $200 \leq T/\text{K} \leq 300$ to the Curie-Weiss law, see Table 1. The measured Curie constants can be compared to the calculated value

$$C_m^{calc} = \frac{2-x}{8}\left(\mu_{so}^{Ni}\right)^2 + \frac{x}{8}(\mu_{so}^{Cu})^2,$$

where μ_{so}^{Ni} and μ_{so}^{Cu} represent the spin–only effective moments of Ni^{2+} and Cu^{2+}. Figure 1(c) shows χ_{FC} (T) of $CaLa_2Ni_{2-x}Cu_xWO_9$ (x = 0 [8], 0.25 and 0.5), with the inset showing the shift

in the magnetic transition temperature at around 30 – 35 K when x increases from 0 to 0.25. The field-dependence of the magnetisation of $CaLa_2Ni_{2-x}Cu_xWO_9$ (x = 0.25 and 0.5) is shown in Figure 2. Neither compound shows clear hysteresis at temperatures above 5 K although $M(H)$ is nonlinear below 220 K. Hysteresis is, however, present for $0 \leq x \leq 0.5$ at 5 K, see Figure 2(c) although $M(H)$ remains unsaturated when H = 50 kOe. The remanent magnetisation, M_R, increases with x in the $CaLa_2Ni_{2-x}Cu_xWO_9$ series whereas the coercive field, H_C, is smallest when x = 0.5, see Table 1. All the magnetometry parameters, together with the corresponding parameters of Cu-free $CaLa_2Ni_2WO_9$ [8], are listed in Table 1. The temperature and frequency dependence of the ac molar susceptibilities of the two Cu-containing perovskites are shown in Figure 3. The maximum of $\chi'(T)$ of $CaLa_2Ni_{1.75}Cu_{0.25}WO_9$ shows only a weak frequency dependence and the general shape mimics that of the dc magnetic susceptibility; a single maximum is observed at ~35 K indicating that only one magnetic transition is present. However, the imaginary component, which has an additional, relatively-broad local maximum at 55 K, suggests that this composition undergoes two transitions. Conversely, the real component χ' of $CaLa_2Ni_{1.5}Cu_{0.5}WO_9$ is strongly frequency dependent, as is χ''. The behaviour of $\chi''(T)$ at ~80 K suggests the magnetic transition temperature is frequency dependent, but this variation is not apparent in χ'.

The neutron diffraction data collected from both samples at room temperature were consistent with the corresponding X-ray data and could thus be accounted for using a monoclinic structural model with a disordered arrangement of Ca^{2+} and La^{3+} cations on one 4-fold site, three crystallographically-distinct oxide ions, each on a 4-fold, site, and two 2-fold six-coordinate sites each accommodating a mixture of Ni^{2+}, Cu^{2+} and W^{6+} cations. On the basis of the results of preliminary refinements, the distribution of these cations over the two sites was refined with the assumption that there was no ordering of the Cu^{2+} and Ni^{2+} cations, that is the ratio of Ni^{2+}:Cu^{2+} on each site is the same as the overall Ni^{2+}:Cu^{2+} ratio in the sample. The

results presented in Table 2 show that the majority of the diamagnetic W^{6+} cations occupy the 2*d* site, leaving the 2*c* site occupied almost exclusively by Ni^{2+} and Cu^{2+}; this is consistent with the shorter mean metal-to-oxygen distance found at the former site, see Table 3. The fits to the neutron diffraction patterns collected at room temperature are shown in Figure 4 and the structure is drawn in Figure 5.

Further diffraction patterns were collected from $CaLa_2Ni_{1.75}Cu_{0.25}WO_9$ at 150, 100, 50, 25 and 1.6 K. No magnetic Bragg scattering was apparent in any of these patterns, which could all be accounted for using the room-temperature structural model. These data will not be discussed further. However, when a similar sequence of measurements was performed on $CaLa_2Ni_{1.5}Cu_{0.5}WO_9$ additional Bragg intensity was clearly observed at and below 130 K, but not at 145 K and above. A full analysis of the data collected at 145 K was carried out, albeit with the cation distribution fixed to that determined at room temperature. In order to avoid correlation effects between the atomic coordinates and the magnetic moment, the former were then held constant during the analysis of data collected from the magnetic phase although the unit cell parameters and the displacement parameters were allowed to vary freely. The magnetic scattering could be accounted for by a G-type spin arrangement with the atomic moments aligned along [001]. The moments on nearest-neighbour 2*c* and 2*d* sites align antiparallel, see Figure 5, with the different occupancy factors of the magnetic cations leading to ferrimagnetism as previously reported in the case of $LaSr_2Cr_2SbO_9$ [2]. The fit to the diffraction pattern collected at 1.6 K is shown in Figure 6. The mean ordered magnetic moment refined to a value of 0.774(5) μ_B per magnetic cation (Ni^{2+} or Cu^{2+}). Analysis of the diffraction patterns collected at 50 K resulted in the same value, within error, but a reduced moment (0.580(7) μ_B) was found at 90 K. With magnetic occupation factors of 0.962 and 0.371 at the 2*c* and 2*d* sites, respectively, an atomic moment of 0.774(5) μ_B corresponds to a saturation magnetisation of 0.68 μ_B per formula unit of $CaLa_2Ni_{1.5}Cu_{0.5}WO_9$ at 1.6 K.

Discussion

We have shown that $CaLa_2Ni_{2-x}Cu_xWO_9$ can be prepared for $x \leq 0.5$; it may be possible to increase the concentration of Cu^{2+} further by making modifications to the synthesis protocol. Although our structural model gives a good account of the observed diffraction patterns we note that the values of the atomic displacement parameters of all the atoms, see Table 2, are large at room temperature and that most remain relatively large at 1.6 K, suggesting that the atoms undergo significant static displacements away from their mean positions. This local disorder, which increases with increasing copper content, is a consequence of the fact that the cation sites are occupied by two or three different cation species, each with its own coordination requirements. Although the solid solution is essentially isostructural with the Cu-free $x = 0.0$ composition [8] there is a difference in the distribution of the three distinct 2*c* – O and 2*d* – O bond lengths; in the solid solution the bonds to O3 at the copper-rich 2*c* site are extended significantly and those at the tungsten-rich 2*d* site are contracted. In the case of $CaLa_2Ni_2WO_9$ no significant, equivalent contraction could be recognised in the data. The increase in the distortion of the octahedra of oxide ions around these two sites can be attributed to the introduction of a Jahn-Teller cation, Cu^{2+}, that would have a degenerate $3d^9$ electronic ground state in a regular octahedral environment; a comparable distortion is present in the cation-ordered perovskite Sr_2CuWO_6 [13, 14]. This effect is less clear in the case of $La_3Ni_{2-x}Cu_xNbO_9$ [7], wherein the Cu^{2+} cations were found to be unevenly distributed over the 2*c* and 2*d* sites; at a substitution level of $x = 0.25$ there was no evidence for the presence of Cu^{2+} on the niobium-rich site.

The magnetic properties of $CaLa_2Ni_{1.75}Cu_{0.25}WO_9$ are similar to those of the copper-free parent composition. The magnetometry and neutron diffraction data suggest that both behave as a spin glass at low temperatures and their transition temperatures are similar. This provides a further

contrast with the niobium-based system wherein $La_3Ni_{1.75}Cu_{0.25}NbO_9$ showed G-type ferrimagnetic ordering below 90 K. However, $CaLa_2Ni_{1.5}Cu_{0.5}WO_9$ does order as a ferrimagnet, see Figures 1 and 3, with a transition temperature of 120 K, similar to that determined for $La_3Ni_{1.5}Cu_{0.5}NbO_9$ and considerably higher than the Néel temperatures of Ca_2NiWO_6 (56 K [15]), Sr_2CuWO_6 (24 K [16]), and Sr_2NiWO_6 (59 K [17]). The measured Curie constants of $CaLa_2Ni_{2-x}Cu_xWO_9$ in the paramagnetic region, see Table 1, do not agree well with the values predicted by the spin-only model, suggesting that significant short-range magnetic coupling is present well above the transition temperature. The large, positive values of the Weiss constant are consistent with the idea that this involves antiferromagnetic coupling of unequally populated sublattices and, consequently, the development of ferrimagnetic regions. The temperature dependence of the ac susceptibility of the $x = 0.25$ sample, see Figure 3(a) reveals complexities above the transition temperature in the range $40 < T/\mathrm{K} < 90$ that are not apparent in the corresponding dc data. Further work will be necessary before these can be elucidated.

The ordered magnetic moment per magnetic cation determined by neutron diffraction is smaller than might have been expected for either Ni^{2+} or Cu^{2+} alone. This might suggest that not all of the cations participate in the long-range ordering at 1.6 K, which would be consistent with the failure of $M(H)$ to saturate in a field of 50 kOe, see Figure 2. Alternatively, it might be attributable to the presence of spin-ordered domains that are too small to contribute to the diffraction pattern; the reduced ordered moment observed in $LaSr_2Cr_2SbO_9$ [2] has previously been shown by muon spin relaxation measurements [18] to be a consequence of a domain structure that is controlled by the cation disorder. The magnetisation per formula unit of $CaLa_2Ni_{1.5}Cu_{0.5}WO_9$ predicted from the diffraction measurements is in reasonable, but not good, agreement with the remanent magnetisation measured by magnetometry.

Replacing Ni^{2+} cations in $Ca_2LaNi_2WO_9$ with Cu^{2+} cations introduces $3d^9$ cations into a $3d^8$ system and results in a pseudo-tetragonal distortion of the coordination polyhedra around the six-coordinate sites and increased static displacements of the atoms away from their mean positions. When 25 % of the Ni^{2+} cations have been substituted these changes in the crystal and electronic structures change the relative strengths of the different magnetic superexchange interactions (nearest-neighbour, next-nearest-neighbour etc.) sufficiently to convert a spin glass with T_g = 32 K into a ferrimagnet with T_c = 120 K. The adoption of a G-type magnetic structure shows that the dominant interaction in the latter is the nearest-neighbour 2*c* – O – 2*d* superexchange that occurs over a distance of ~4 Å. In the copper-free composition this interaction is presumably frustrated by competition from next-nearest-neighbour interactions over a distance of ~5.5 Å and pseudo-linear interactions along a pathway that is ~8 Å in length. The former has been shown to be the dominant antiferromagnetic superexchange pathway in $SrLaNiSbO_6$ [19] where it results in an A-type, rather than a G-type, magnetic structure and the latter has been shown to be dominant in Sr_2CuWO_6 [13], Sr_2NiWO_6 [20] and Ca_2NiWO_6 [15]. Which of these two interactions is stronger depends on whether the *d* orbitals of the diamagnetic six-coordinate cation are energetically available to play a role in the superexchange and the longer pathway would therefore be expected to be the stronger in $CaLa_2Ni_{2-x}Cu_xWO_9$, as it is in the other compounds containing d^0 W^{6+} cations. However, this interaction will always be weaker than the Ni – O – Ni superexchange that occurs in $CaLa_2Ni_2WO_9$ when neighbouring 2c and 2*d* sites are both occupied by Ni^{2+}. This suggests that in $CaLa_2Ni_2WO_9$ the frustration of the 4 Å interaction must also be at least partially attributable to the 5.5 Å Ni – Ni interaction, which is almost always fulfilled between pairs of nickel-rich 2c sites and also by some 2*d* pairs. These arguments lead us to conclude that the spin-glass to ferrimagnet transition occurs because the introduction of Cu^{2+} weakens the 8 Å and 5.5 Å superexchange pathways faster than the 4 Å pathway. This can be attributed either

to the difference in the electron configurations of Cu^{2+} and Ni^{2+} or to the tendency of short-range structural disorder to weaken longer pathways more than short pathway. In the case of the $La_3Ni_{2-x}Cu_xNbO_9$ system the change from spin glass to ferrimagnet is complete when x = 0.25 [7]. The relative robustness of the former state in the tungsten analogue might be due to an increase, compared to the case of niobium, in the mixing of the tungsten *d* orbitals and the oxide *p* orbitals and hence a strengthening of the 8 Å pathway; the magnitude of this effect will be partly determined by the increased mean acidity of the A-site cations (Ca^{2+} *vs* La^{3+}). The change in the Cu^{2+}/Ni^{2+} distribution over the two six-coordinate sites might also be a factor. Further experimental data will have to be collected before these issues can be resolved.

Conclusion

The replacement of Ni^{2+} in $CaLa_2Ni_2WO_9$ by Cu^{2+} causes a remarkable change in the magnetic properties of the material. The copper-free composition behaves as a spin-glass below 32 K whereas $CaLa_2Ni_{1.5}Cu_{0.5}WO_9$ is ferrimagnetic below 120 K. The change in magnetic behaviour can be attributed to the difference in the electronic structures of Cu^{2+} and Ni^{2+} and to the differential disruption of the superexchange pathways that is caused by the increase in structural disorder that accompanies the cation substitution.

Acknowledgments

We thank the EPSRC for financial support under grant EP/M018954/1 and the STFC for the award of beamtime at the ISIS neutron source. CMC thanks the Croucher Foundation and Oxford University for a graduate scholarship. We are grateful to P. Manuel for experimental assistance at ISIS.

References

[1] C.M. Chin, P.D. Battle, E.C. Hunter, M. Avdeev, M. Hendrickx, J. Hadermann, J. Solid State Chem. 273 (2019) 175-185.
[2] E.C. Hunter, P.D. Battle, R. Paria Sena, J. Hadermann, J. Solid State Chem. 248 (2017) 96-103.
[3] C.M. Chin, P.D. Battle, S.J. Blundell, E. Hunter, F. Lang, M. Hendrickx, R.P. Sena, J. Hadermann, Journal of Solid State Chemistry 258 (2018) 825-834.
[4] M.T. Anderson, K.B. Greenwood, G.A. Taylor, K.R. Poeppelmeier, Progress in Solid State Chemistry 22 (1993) 197-233.
[5] S. Vasala, M. Karppinen, Progress in Solid State Chemistry 43 (2015) 1-36.
[6] C.M. Chin, P.D. Battle, A.L. Goodwin, A. Wildes, Journal of Solid State Chemistry 278 (2019).
[7] C.M. Chin, P.D. Battle, E.C. Hunter, M. Avdeev, M. Hendrickx, J. Hadermann, Journal of Solid State Chemistry 276 (2019) 164-172.
[8] C.M. Chin, R. Paria Sena, E.C. Hunter, J. Hadermann, P.D. Battle, Journal of Solid State Chemistry 251 (2017) 224-232.
[9] H.M. Rietveld, Journal of Applied Crystallography 2 (1969) 65 - 71.
[10] A.C. Larson, R.B. von-Dreele *General Structure Analysis System (GSAS)* Los Alamos National Laboratories LAUR 86-748 1994
[11] L.C. Chapon, P. Manuel, P.G. Radaelli, C. Benson, L. Perrott, S. Ansell, N.J. Rhodes, D. Raspino, D. Duxbury, E. Spill, J. Norris, Neutron News 22 (2011) 22-25.
[12] A.A. Coelho, Journal of Applied Crystallography 51 (2018) 210-218.
[13] S. Vasala, M. Avdeev, S. Danilkin, O. Chmaissem, M. Karppinen, Journal of Physics-Condensed Matter 26 (2014) 96001-96001.
[14] Y.H. Xu, S.S. Liu, N.R. Qu, Y.L. Cui, Q.Q. Gao, R.N. Chen, J. Wang, F.M. Gao, X.F. Hao, Journal of Physics-Condensed Matter 29 (2017).
[15] M.J. Martinez-Lope, J.A. Alonso, M.T. Casais, M.T. Fernandez-Diaz, Z. Naturforschung 58b (2003) 127 - 132.
[16] H.C. Walker, O. Mustonen, S. Vasala, D.J. Voneshen, M.D. Le, D.T. Adroja, M. Karppinen, Physical Review B 94 (2016) 4411-4411.
[17] S. Nomura, T. Nakagawa, J. Phys. Soc. Japan 21 (1966) 1679 - 1684.
[18] E.C. Hunter, P.D. Battle, S.J. Blundell, C.V. Topping, F.K.K. Kirschner, F. Lang, Journal of Solid State Chemistry 279 (2019).
[19] M.P. Attfield, P.D. Battle, S.K. Bollen, T.C. Gibb, R.J. Whitehead, Journal of Solid State Chemistry 100 (1992) 37.
[20] Y. Todate, Journal of Physics and Chemistry of Solids 60 (1999) 1173-1175.

Table 1. Magnetic parameters of $CaLa_2Ni_{2-x}Cu_xWO_9$ (x = 0, 0.25 and 0.5)

x	C_m^{calc}	C_m	θ_W	H_C	M_R	T_C	T_{MAX}	M_O*
	cm^3 K mol^{-1}	cm^3 K mol^{-1}	K	kOe	μ_B	K	K	μ_B
0	2.00	1.24(1)	119(3)	1.5	0.04	32	32	n/a
0.25	1.84	1.03(2)	153(5)	1.2	0.15	35	35	n/a
0.5	1.69	1.05(1)	170(3)	0.4	0.42	120	60	0.774(5)

Data for $CaLa_2Ni_2WO_9$ are taken from [8].
*Mean ordered moment per magnetic cation

Table 2 Structural parameters of $CaLa_2Ni_{2-x}Cu_xWO_9$ at room temperature and 1.6 K, space group $P2_1/n$

		x = 0.25		x = 0. 5	
		Room temp.	1.6 K	Room temp.	1.6 K*
a/Å		5.53343(3)	5.52122(4)	5.53688(9)	5.52429(4)
b/Å		5.58552(3)	5.58337(4)	5.59641(8)	5.59466(4)
c/Å		7.84132(3)	7.82736(4)	7.8458(1)	7.83135(4)
β/º		89.999(3)	89.993(4)	90.001(3)	89.998(3)
V/Å^3		242.352(2)	241.294(3)	243.116(6)	242.040(3)
R_{wp}/%		2.9	3.7	2.8	3.45
χ^2		0.9	1.0	0.5	0.6
Ca/La	x	0.4899(3)	0.4904(4)	0.4945(4)	0.4954(4)
4e(x, y, z)	y	0.4616(2)	0.4600(2)	0.4596(2)	0.4588(2)
	z	0.2561(4)	0.2543(5)	0.2503(5)	0.2498(5)
	U_{iso}/Å^2	0.0303(2)	0.0245(3)	0.0401(4)	0.0355(2)
	Ca occupancy	0.3333	0.3333	0.3333	0.3333
	La occupancy	0.6666	0.6666	0.6666	0.6666
Ni/Cu/W1	U_{iso}/Å^2	0.01928(8)	0.016(1)	0.0242(9)	0.0174(6)
2c(0, ½, 0)	Ni occupancy	0.842(4)	0.842(4)	0.719(4)	0.719
	Cu occupancy	0.120(1)	0.120(1)	0.240(1)	0.240
	W occupancy	0.038(5)	0.038(5)	0.041(5)	0.041
Ni/Cu/W2	U_{iso}/Å^2	0.009(1)	0.011(1)	0.020(1)	0.0202(8)
2d(½, 0, 0)	Ni occupancy	0.325(4)	0.325	0.281(4)	0.281
	Cu occupancy	0.046(1)	0.046	0.094(1)	0.094
	W occupancy	0.629(5)	0.629	0.625(5)	0.625
O1	x	0.7885(4)	0.7909(5)	0.7941(5)	0.7954(5)
4e(x, y, z)	y	0.7850(4)	0.7864(5)	0.7889(5)	0.7886(5)
	z	-0.0435(4)	-0.0445(5)	-0.0415(5)	-0.0427(5)
	U_{iso}/Å^2	0.011(2)	0.011(2)	0.022(3)	0.014(2)
O2	x	0.7037(4)	0.7051(5)	0.7078(5)	0.7085(5)
4e(x, y, z)	y	0.2918(3)	0.2911(4)	0.2890(5)	0.2905(5)
	z	-0.0333(4)	-0.0347(5)	-0.0366(5)	-0.0359(5)
	U_{iso}/Å^2	0.013(2)	0.006(2)	0.032(3)	0.034(2)
O3	x	0.5803(2)	0.5832(2)	0.5813(2)	0.5827(2)
4e(x, y, z)	y	0.0171(2)	0.0186(3)	0.0173(2)	0.0179(3)
	z	0.2317(3)	0.2316(4)	0.2286(4)	0.2286(4)
	U_{iso}/Å^2	0.0283(4)	0.0270(6)	0.0346(6)	0.0308(3)

* The atomic coordinates listed here, together with their esds, are those determined from data collected at 145 K. These coordinates were held constant during the analysis of data collected at 1.6 K.

Table 3 Selected bond lengths (Å) and bond angles (deg.) in $CaLa_2Ni_{2-x}Cu_xWO_9$ at room temperature

	$x = 0.25$	$x = 0.5$
Ca/La – O1	2.391(3)	2.426(4)
Ca/La – O1	2.655(3)	2.678(4)
Ca/La – O1	2.749(4)	2.739(5)
Ca/La – O2	2.469(3)	2.457(5)
Ca/La – O2	2.691(3)	2.692(4)
Ca/La – O2	2.729(4)	2.718(5)
Ca/La – O3	2.401(2)	2.377(2)
Ca/La – O3	2.540 (2)	2.527(2)
2*c* – O1	2.005(2) x 2	2.000(3) x 2
2*c* – O2	2.027(2) x 2	2.019(3) x 2
2*c* – O3	2.153(2) x 2	2.184(3) x 2
2*d* – O1	2.027(2) x 2	2.042(3) x 2
2*d* – O2	1.999(2) x 2	2.011(3) x 2
2*d* – O3	1.872(2) x 2	1.847(3) x 2
O1 – 2*c* – O2	92.21(8)	90.5(1)
O1 – 2*c* – O3	90.60(9)	90.3(1)
O2 – 2*c* – O3	90.89(9)	90.0 (1)
O1 – 2*d* – O2	90.98(8)	90.7(1)
O1 – 2*d* – O3	90.37(8)	90.6(1)
O2 – 2*d*– O3	92.79(9)	92.5(1)

Figure Captions

Figure 1 The temperature variation of the dc molar magnetic susceptibilities of $CaLa_2Ni_{2-x}Cu_xWO_9$. The red, blue and green symbols represent the compositions x = 0, 0.25 and 0.5 respectively.

Figure 2 The magnetisation per formula unit (f.u.) of $CaLa_2Ni_{2-x}Cu_xWO_9$ as a function of magnetic field and temperature. The red, blue and green symbols represent the compositions x = 0, 0.25 and 0.5 respectively.

Figure 3 The field and temperature dependence of the ac molar susceptibilities of (a) $CaLa_2Ni_{1.75}Cu_{0.25}WO_9$ and (b) $CaLa_2Ni_{1.5}Cu_{0.5}WO_9$.

Figure 4 Observed and calculated neutron powder diffraction profiles of $CaLa_2Ni_{2-x}Cu_xWO_9$ (x = 0.25 and x = 0.5) at room temperature; a difference curve is shown and reflection positions are marked.

Figure 5 Crystal structure of $CaLa_2Ni_{1.5}Cu_{0.5}WO_9$; red circles represent Ca^{2+} and La^{3+} cations, 2*c* and 2*d* sites coordinated by six oxide ions are represented by blue and green octahedra. At low temperatures the magnetic moments of the cations within adjacent, vertex-sharing octahedra align antiparallel.

Figure 6 Observed and calculated neutron powder diffraction profiles of $CaLa_2Ni_{2-x}Cu_xWO_9$ (x = 0.25 and x = 0.5) at 1.6 K; a difference curve is shown and reflection positions are marked. In the case of magnetic x = 0.5, blue (black) reflection markers correspond to the space group $P2_1/n$ (P-1). The peak with d ~4.5 Å has the largest magnetic component.

(a)

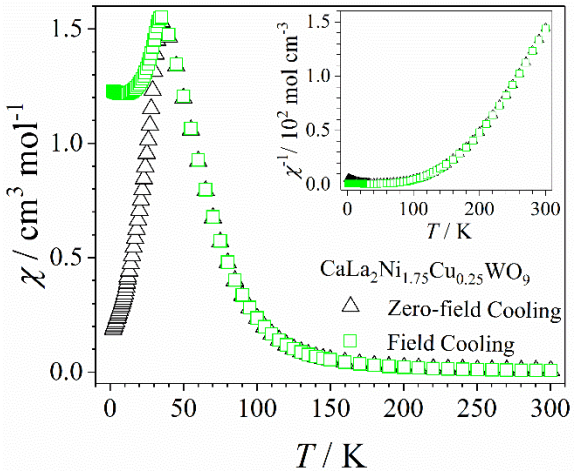
χ / cm³ mol⁻¹
T / K
χ⁻¹ / 10² mol cm⁻³
CaLa₂Ni₁.₇₅Cu₀.₂₅WO₉
Zero-field Cooling
Field Cooling

(b)

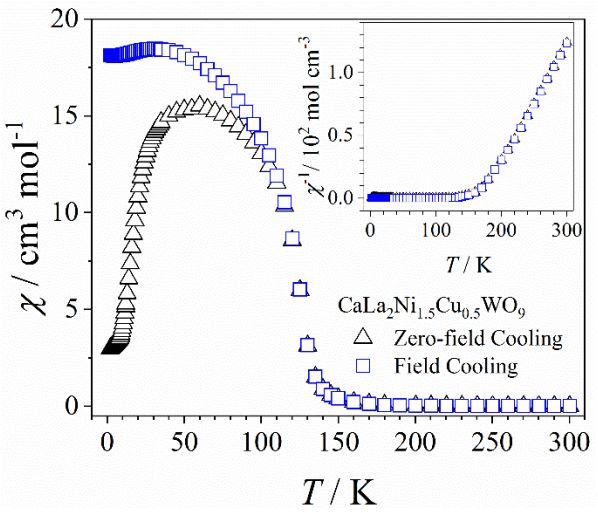
χ / cm³ mol⁻¹
T / K
χ⁻¹ / 10² mol cm⁻³
CaLa₂Ni₁.₅Cu₀.₅WO₉
Zero-field Cooling
Field Cooling

(c)

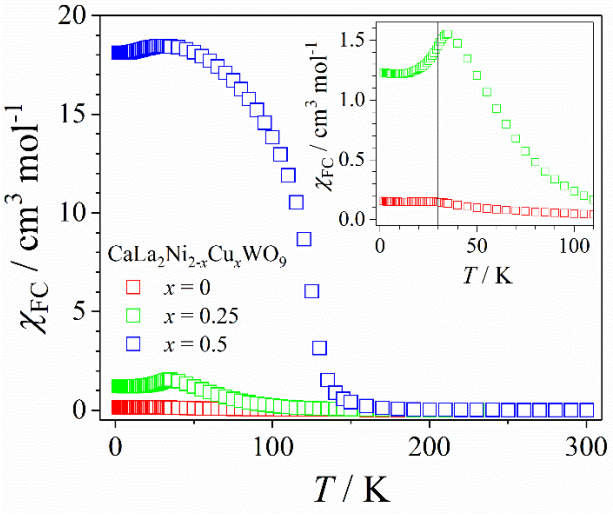
χFC / cm³ mol⁻¹
T / K
χFC / cm³ mol⁻¹
CaLa₂Ni₂₋ₓCuₓWO₉
x = 0
x = 0.25
x = 0.5

Figure 1.

(a)

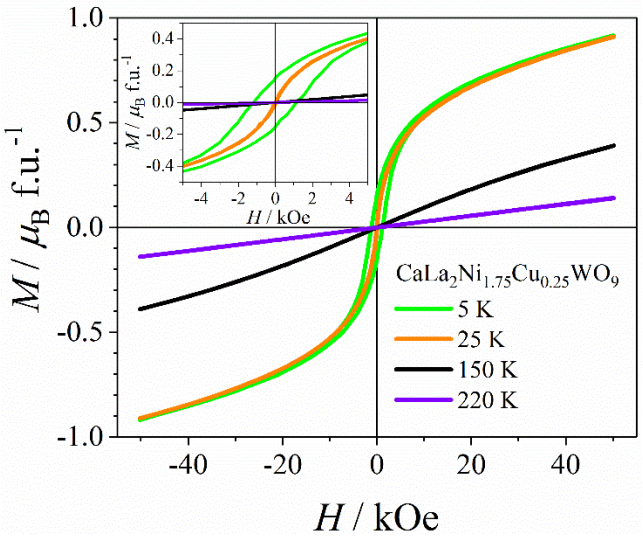
1.0
0.5
0.0
-0.5
-1.0
-40
-20
0
20
40
H / kOe
M / μB f.u.-1
0.4
0.2
0.0
-0.2
-0.4
-4
-2
0
2
4
CaLa2Ni1.75Cu0.25WO9
5 K
25 K
150 K
220 K

(b)

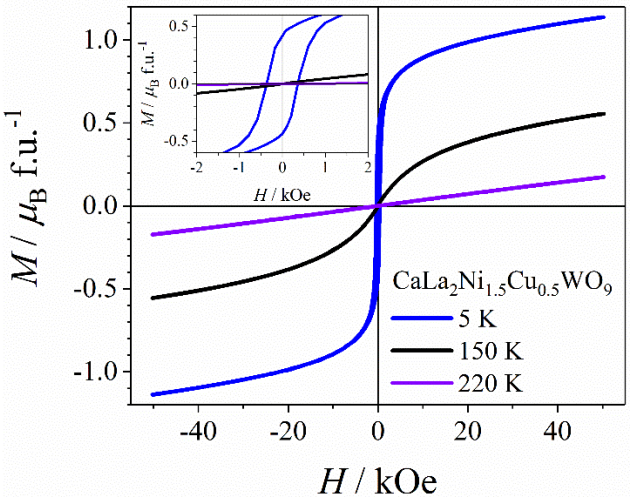
1.0
0.5
0.0
-0.5
-1.0
-40
-20
0
20
40
H / kOe
M / μB f.u.-1
0.5
0.0
-0.5
-2
-1
0
1
2
CaLa2Ni1.5Cu0.5WO9
5 K
150 K
220 K

(c)

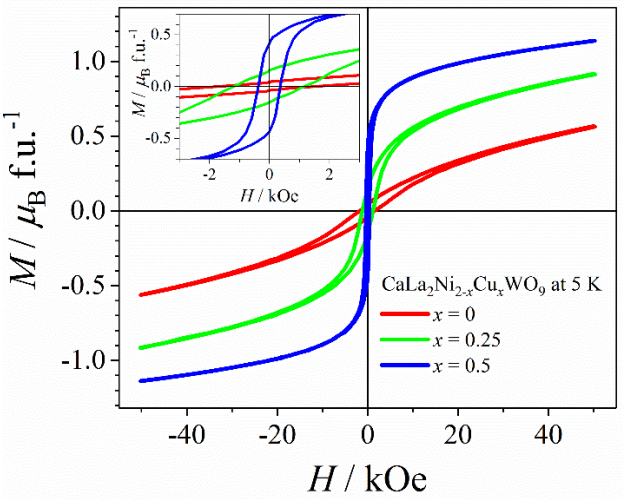
1.0
0.5
0.0
-0.5
-1.0
-40
-20
0
20
40
H / kOe
M / μB f.u.-1
0.5
0.0
-0.5
-2
0
2
CaLa2Ni2-xCuxWO9 at 5 K
x = 0
x = 0.25
x = 0.5

Figure 2.

(a)

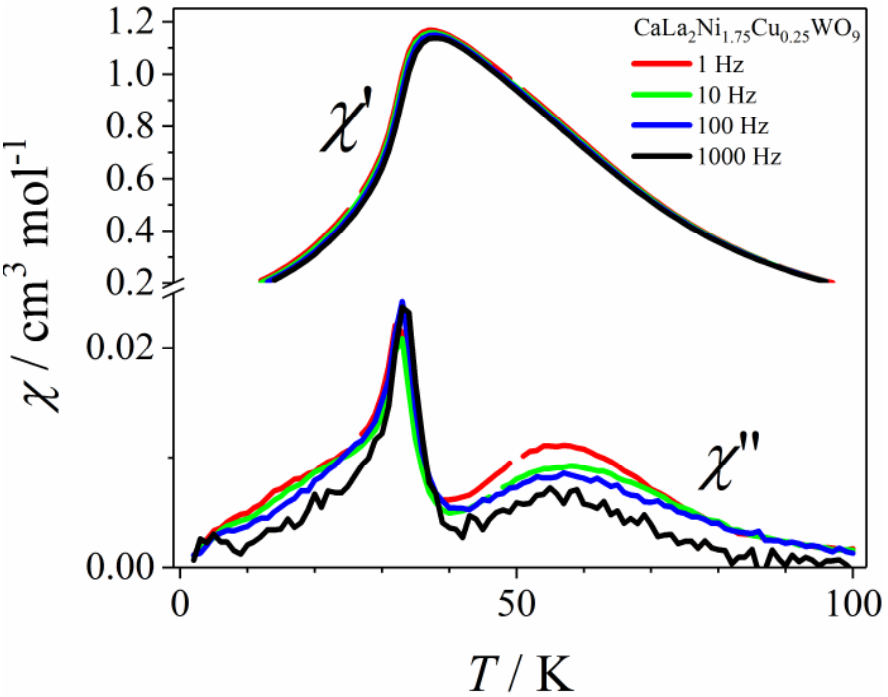
CaLa2Ni1.75Cu0.25WO9
1 Hz
10 Hz
100 Hz
1000 Hz
χ'
χ''
χ / cm3 mol-1
T / K

(b)

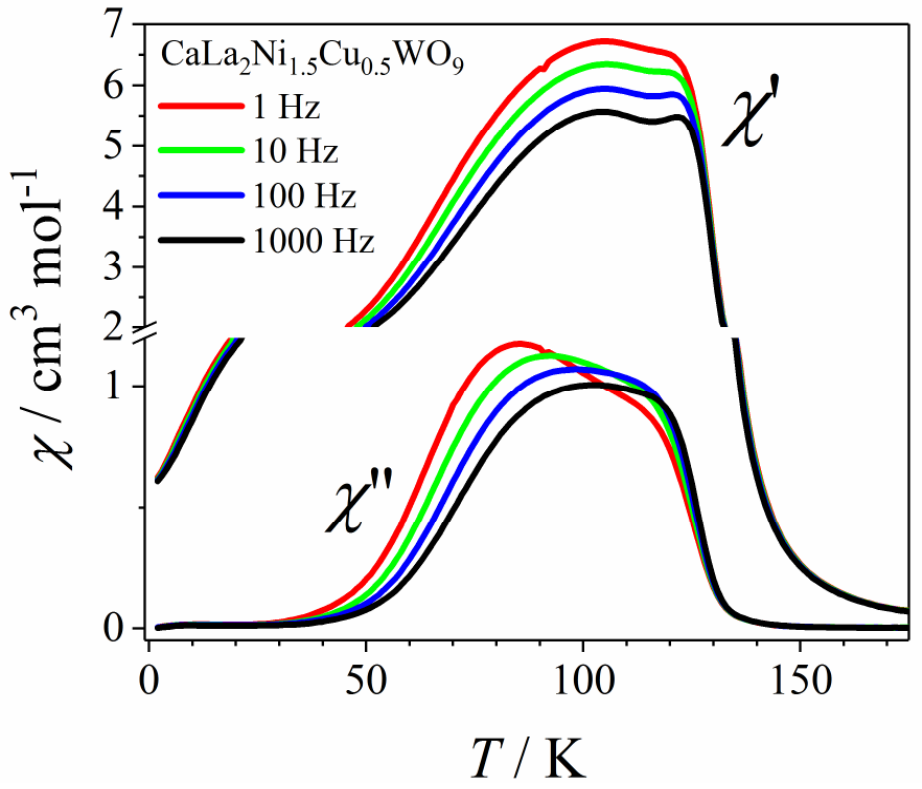
CaLa2Ni1.5Cu0.5WO9
1 Hz
10 Hz
100 Hz
1000 Hz
χ'
χ''
χ / cm3 mol-1
T / K

Figure 3.

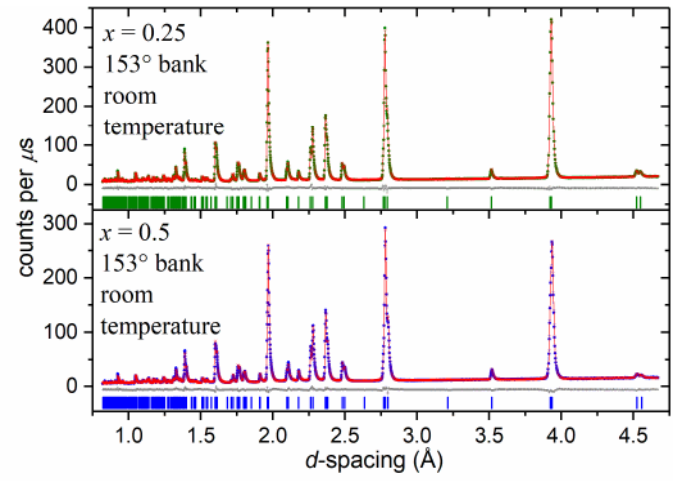

Figure 4

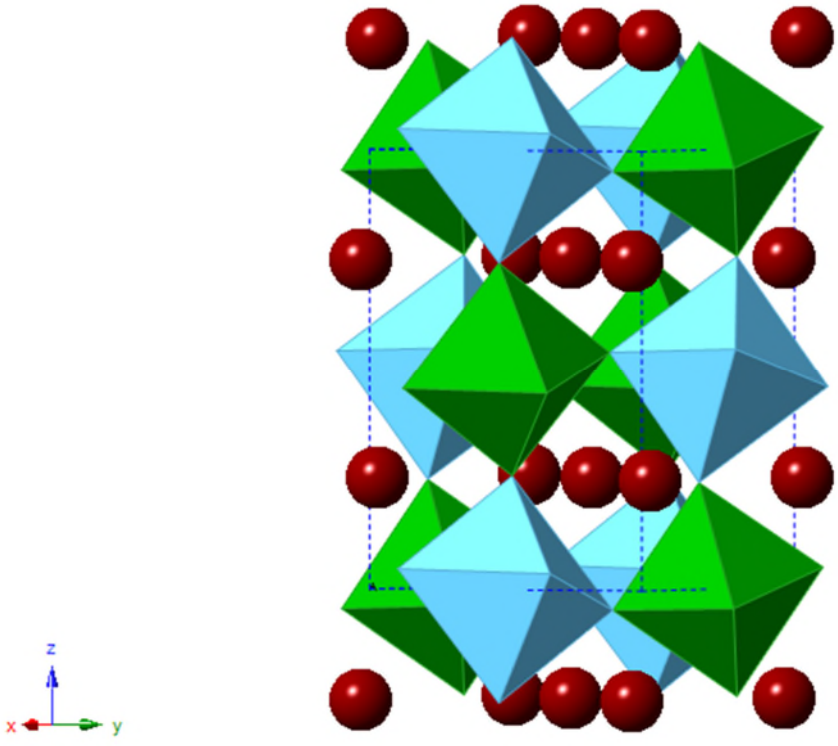

Figure 5

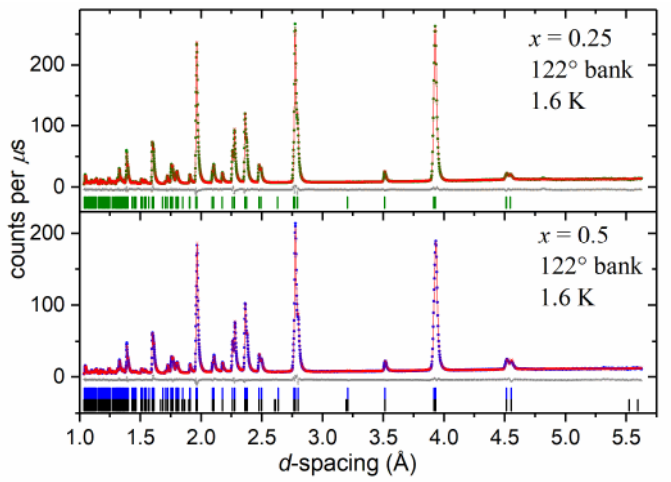

Figure 6